J Nanopart Res (2020) 22: 72
https://doi.org/10.1007/s11051-020-04798-7

RESEARCH PAPER

Transferrin-conjugated doxorubicin-loaded PLGA nanoparticles with pH-responsive behavior: a synergistic approach for cancer therapy

Laís E. Scheeren · Daniele R. Nogueira-Librelotto · Letícia B. Macedo · Josiele M. de Vargas · Montserrat Mitjans · M. Pilar Vinardell · Clarice M. B. Rolim

Received: 31 October 2019 / Accepted: 28 February 2020 / Published online: 14 March 2020

Abstract Doxorubicin (DOX) is an efficient chemotherapeutic agent widely used to treat different types of cancer; however, there is an inherent risk of adverse effects due to its unspecific action in healthy cells. In order to enhance the DOX arrival and accumulation inside the cancerous cells, we have developed DOX-loaded nanoparticles (NPs) using the biocompatible polymer poly(lactic-*co*-glycolic acid) (PLGA). pH sensitivity was achieved by incorporation of the surfactant, 77KS, while poloxamer was explored as stabilizer and chemosensitizer. The protein transferrin (Tf) was conjugated to the NPs with the role to actively targeting them to the cancerous cells. The nanoprecipitation method yielded NPs with size about 100 nm, with polydispersity index around 0.20 and a negative zeta potential. Transmission electron microscopy and infrared spectroscopy confirmed the shape and the functional groups presence. DOX release from the NPs followed a control and pH-sensitive pattern, allowing accelerated DOX release in acidic conditions. Through the hemolysis assay, using the erythrocyte as a model for the endosomal membrane, it was evidenced the pH-sensitive membranolytic behavior of the NPs. Furthermore, the NPs were safe and compatible with blood. Finally, the formulations were applied to tumor and non-tumor cell lines, HeLa and HaCaT, respectively. Over 72 h of incubation, the Tf-conjugated NPs induced a notable reduction in HeLa cell growth and were able to protect the HaCaT cells from the DOX unspecific cytotoxicity. The results suggest that the dual-active targeting promoted by 77KS and Tf is a promising platform to overcome the side effects of conventional chemotherapeutic drugs and nontargeted nanosystems.

Keywords Transferrin · Active targeting · pH-sensitivity · Cancer treatment · Lysine-based surfactant · Doxorubicin · Nanomedicine

L. E. Scheeren · D. R. Nogueira-Librelotto (✉) · L. B. Macedo · J. M. de Vargas · C. M. B. Rolim (✉)
Departamento de Farmácia Industrial, Universidade Federal de Santa Maria, Av. Roraima 1000, Santa Maria, RS 97105-900, Brazil
e-mail: daniele.rubert@gmail.com
e-mail: clarice.rolim@ufsm.br

L. E. Scheeren · D. R. Nogueira-Librelotto · L. B. Macedo · C. M. B. Rolim
Programa de Pós-Graduação em Ciências Farmacêuticas, Universidade Federal de Santa Maria, Av. Roraima 1000, Santa Maria, RS 97105-900, Brazil

M. Mitjans · M. P. Vinardell
Departament de Bioquimica i Fisiologia, Facultat de Farmacia i Ciències de l'Alimentació, Universitat de Barcelona, Av. Joan XXIII 27-31, 08028 Barcelona, Spain

Introduction

The development of drug delivery systems to encapsulate antineoplastic drugs is a field of nanoscience and nanotechnology research that emerges as an alternative to circumvent the traditional side effects of cancer treatments, improving therapeutic benefits and enhancing

safety (Hare et al. 2017). These systems can be adapted for passive and/or active targeting. To reach the active strategy, several specific ligands to target different cancer sites can be used in the NP structure, such as proteins, peptides, hyaluronic acid, folate, antibodies, aptamer, and carbohydrates (Muhamad et al. 2018). Alternatively and/or synergistically, the endogenous pH stimuli can destabilize the drug-loaded delivery system at specific sites in the body, achieving the potential to overcome the lack of targeting of conventional anticancer modalities (Danhier et al. 2010).

Doxorubicin (DOX) is an antibiotic, produced by the *Streptomyces* bacteria, discovered in the 1960s and used as an antineoplastic drug since then (Barenholz 2012). DOX presents multiple mechanisms of action, but two of them are the most important: (i) induction of DNA damage through interference with topoisomerase II and (ii) free radical generation, strongly related to cardiotoxicity of the anthracyclines (Gewirtz 1999; Thorn et al. 2011). However, the cell exposition to anticancer agents can develop multi-drug resistance (MDR), which is well known for DOX. This form of cell protection can occur by molecular changes such as many membrane efflux pumps, increase drug metabolism enzymes and failure of the cellular apoptotic pathways (AbuHammad and Zhilif 2013). Then, poloxamer, a block-co-polymer, has been studied as a sensitizer agent in drug-resistant tumors, with the ability to preferentially target cancer cells as well as to enhance the proapoptotic signaling (Batrakova and Kabanov 2008; Swider et al. 2018).

Transferrin (Tf) protein is found primarily in the bloodstream. It's highly stable, which may be due to its high content of disulfide bonds (Shen et al. 1992). This protein have the ability to bind, tightly but reversibly, two Fe^{3+} ions, and the presence of specific Tf receptors (TfR) on cells gives it the role of transporting iron and delivery it by receptor-mediated endocytosis (Baker et al. 2002). Some studies have previously described a high level of TfR expression on cancer cells when compared to the normal counterparts (Daniels et al. 2006; Nogueira-Librelotto et al. 2017; Shindelman et al. 1981). It was demonstrated elsewhere that Tf-conjugated poly(lactic-*co*-glycolic acid) (PLGA) NPs, prepared without any drug, are more easily endocytosed by the blood-brain barrier (BBB) and glioma cells (Chang et al. 2009, 2012). Likewise, Tf-modified polymeric NPs containing DOX were able to inhibit the growth of different tumor cell lines (Cui et al. 2013; Tsuji et al. 2013; Zhang et al. 2016). This background places the Tf as an attractive molecule to be included in nanocarriers to deliver the encapsulated drug actively at target cancer cells.

Unlike the normal tissues, which have pH values in the physiological range, the pH of the tumor region (pH_e) and of the lyso-endosomal compartments are generally lower, i.e., 6.5–7.2 and 5.0–6.5, respectively, making the pH a more universal approach for tumor targeting, through pH-sensitive delivery systems (Lee et al. 2007; Tian and Bae 2012). In this context, we have studied a unique and exclusive group of surfactants, achieving great results with its association to NPs encapsulating chemotherapeutic agents (Macedo et al. 2019; Nogueira et al. 2011a, 2013, 2015, 2016; Nogueira-Librelotto et al. 2016; Scheeren et al. 2016; Vives et al. 1999). Among these surfactants, it is important to highlight the 77KS (N^{α},N^{ε}-dioctanoyl lysine with an inorganic sodium counterion), which showed low cytotoxicity and pH-responsive properties when conjugated to unloaded or DOX-loaded chitosan NPs (Nogueira et al. 2011a, b; Nogueira-Librelotto et al. 2016; Scheeren et al. 2016).

The design of a new and effective target delivery system for DOX is necessary to increase the drug concentration in the tumor, as well as to reduce its undesirable effects on normal tissues. In this investigation, PLGA, a biocompatible, biodegradable, and safely administrable polymer approval by the FDA and EMA (Sharma et al. 2016), was used to engineer DOX-loaded NPs, containing poloxamer, the pH-sensitive surfactant 77KS, and the Tf protein as bioactive adjuvants. The NPs were well-characterized and the stability of the NPs was evaluated, along with the discussion of the pH-triggered DOX control release profiles. The hemolysis assay was used to monitor the potential capacity of the NPs to destabilize the endosomal membranes. Finally, the safety of the NPs was evaluated by different blood compatibility assays, while the potential to inhibit the tumor cells growth was investigated through in vitro assays using the cancer cell line, HeLa. In the same way, HaCaT cells were used as a non-tumor cell model in order to assess the potential selectivity of the proposed pH-sensitive Tf-conjugated NPs.

Materials and methods

Materials

Doxorubicin hydrochloride (DOX, declared purity of 98.32%) was obtained from Zibo Ocean International

Trade (Zibo, Shangdong, P.R., China). The surfactant 77KS was obtained as a gift from the *Consejo Superior de Investigaciones Cientificas* (CSIC, Barcelona, Espanha) (Sanchez et al. 2006a, b; Vives et al. 1999). PLGA (Resomer® RG 503H; lactide:glycolide 50:50; 24–38 kDa Mw; acid terminated), Span 80® (sorbitan monooleate), Pluronic® F127, human holo-transferrin, N-hydroxysuccinimide (NHS), and 1-ethyl-3-(3-dimethylaminopropyl) carbodiimine (EDC) were purchased from Sigma-Aldrich (St. Louis, MO, USA). Dulbecco's Modified Eagle's Medium (DMEM), fetal bovine serum (FBS), phosphate buffered saline (PBS), L-glutamine solution (200 mM), trypsin-EDTA solution (170,000 U/L trypsin and 0.2 g/L EDTA), and penicillin-streptomycin solution (10,000 U/mL penicillin and 10 mg/mL streptomycin) were purchased from Lonza (Verviers, Belgium). HemosIL SynthASil and HemosIL RecombiPlasin 2G were from Instrumentation Laboratory Company (Bedford, MA, USA).

Preparation of DOX-PLGA-NPs

DOX-loaded PLGA nanoparticles (DOX-PLGA-NPs) were prepared by a nanoprecipitation method (Fessi et al. 1989). Briefly, DOX (0.01 g) was solubilized in 6 mL of methanol and mixed with PLGA (0.05 g) and Span 80® (0.038 g), both in acetone (30 mL). After 30 min, this organic phase was injected into 50 mL of an aqueous dispersion of 0.005 g of the pH-sensitive surfactant 77KS and 0.15 g of Pluronic® F127, under 530 rpm magnetic stirring at room temperature. The pH of the aqueous phase was adjusted to 8.5 with 1 M NaOH. After 10 min, the acetone, methanol, and excess of water were then eliminated by evaporation under reduced pressure to achieve a final volume of 10 mL, corresponding to 1 mg/mL DOX concentration. This suspension was named DOX-PLGA-NPs. For comparison purposes, suspensions without the drug and/or without 77KS were also prepared (PLGA-NPs and DOX-PLGA-NPs w/o 77KS). The suspensions were prepared in triplicate.

Preparation of Tf-DOX-PLGA-NPs

Tf was conjugated on the surface of DOX-PLGA-NPs by a two-step EDC/NHS activation and grafting method (Cui et al. 2013; Tavano et al. 2014). As the first step, 2.1 mL of the NP suspension (DOX-PLGA-NPs) were incubated under slight stirring at room temperature with EDC (200 μL, 30 mg/mL) and NHS (200 μL, 30 mg/mL) for 3 h to obtain amino-reactive esters from the carboxylic acid terminated of the polymer. At the end of the incubation time, the sample was filtered by Centrisart® 10 kDa MWCO centrifugal ultrafiltration unit (Sulpeco, 2.5 mL maximum sample filtered) at 2000*g* for 40 min to eliminate excess EDC and NHS and nonencapsulated DOX. The ultrafiltrate was collected, and the volume of the NP suspension was adjusted to 2.1 mL with ultrapure water. Following, a Tf water solution (300 μL, 10 mg/mL) was added to the NP suspension and maintained under slight stirring at room temperature for 2 h to complete the Tf conjugation. Finally, the sample was filtered by Centrisart® 100 kDa MWCO centrifugal ultrafiltration unit (Sulpeco) at the same conditions early mentioned to remove nonconjugated protein. The ultrafiltrate was collected and the volume of the NP suspension was adjusted to 2.1 mL with ultrapure water. This suspension was named Tf-DOX-PLGA-NPs.

Characterization of the NPs

Mean particle size, zeta potential and pH

The mean hydrodynamic diameter and the polydispersity index (PDI) were analyzed by dynamic light scattering (DLS) in a Malvern Zetasizer ZS (Malvern Instruments, Malvern, UK). For these measurements, the samples were diluted 500 times in purified water. The zeta potential (ZP) values of the NPs were assessed by determining the electrophoretic mobility at the same equipment after 500 times dilution of the samples in 10 mM NaCl. The pH measurements were verified directly in the NP suspensions, using a calibrated potentiometer (UB-10; Denver Instrument, Bohemia, NY, USA), at room temperature. In particular, the Tf-DOX-PLGA-NPs were characterized for the rate of protein conjugation using a commercial kit (BioRad® assay, CA, USA) based on the Bradford dye-binding procedure (Bradford 1976), following the manufacturer protocol. Each measurement was performed at least three times at 595 nm using a double-beam UV-Vis spectrophotometer (UV-1800, Shimadzu, Japan).

Morphological analysis

The morphology of the NPs was analyzed by transmission electron microcopy (TEM). The samples were

adsorbed onto carbon-coated copper grids. They were negatively stained by floating the grids on drops of pH 6.1 phosphotungstic acid. The grids were observed in a Jeol TEM J1010 (JEOL, Japan) electron microscope and the images were acquired at 80 kV with a 1 k × 1 k CCD Megaview camera.

Drug content and encapsulation efficiency

The drug content (DC) and encapsulation efficiency (EE%) were quantified using a high performance liquid chromatography (HPLC) method, which was validated following a previously published procedure (Scheeren et al. 2017), with some modifications. The system consisted of a HPLC Shimadzu (Kyoto, Japan) equipped with a SPD-M20A photodiode array detector (PDA), LC-20AT pump, DGU-20A5 degasser, SIL 20A auto sampler, CBM-20A system controller, LC Solution software (version 1.24 SP1), and a column RP-18 (250 mm × 4.6 × 5 μm, Zorbax Eclipse Plus, Agilent Technologies) with a guard column C_{18} (4.0 × 3.0 mm, Cartridges, Phenomenex). The mobile phase was composed of water pH 3.0 acidified with glacial acetic acid and acetonitrile (70:30, v/v) at a flow rate of 1.0 mL/min. The sample injection volume was 20 μL and the detection wavelength set at 254 nm. The method was validated according the official guideline ICH (ICH, Q2 R1 2005).

The DC was determined after the drug extraction from the NPs using acetonitrile (1:3, v/v) in ultrasound for 10 min at 40 °C followed by 2 min of vortex agitation and compared to a DOX reference solution. The drug EE% was determined by ultrafiltration/centrifugation technique using Amicon Ultra 0.5 Centrifugal Filters (10,000 Da MWCO, Millipore), by adding 300 μL of DOX-PLGA-NPs into this apparatus and submitting it to 10,000 rpm for 20 min in Sigma 2-16P centrifuge (Sigma, Germany). The calculation was made according to the following equation:

$$EE\% = 100\,x\,\frac{(Dc - Df)}{Dc},$$

where *Dc* is the total drug content and *Df* is the free DOX quantified in the Amicon ultrafitrate.

Fourier-transformed infrared spectroscopy

The interactions between the drug and other components of NP matrix were investigated by Fourier-transformed infrared (FT-IR) spectroscopy. Raw material and the lyophilized NPs were recorded from 4000 to 400 cm^{-1} using a Bruker Tensor 27 spectrophotometer (Bruker Optik, Ettlingen, Germany) with compressed KBr disk method.

In vitro drug release

In vitro release studies were performed according to the dialysis bag method (Nothnagel and Wacker 2018). The closed bag containing 1 mL of NP suspension was soaked into a glass beaker containing 100 mL of phosphate buffered saline (PBS) with pH adjusted to 7.4, 6.6, or 5.4. This process was performed separately for each pH during 24 h, at 37 °C under gentle magnetic stirring. The dialysis bag (Sigma-Aldrich, molecular weight cutoff 14,000 Da) is able of retain the nanoparticle and allow only free drug to reach the release medium. At specific time intervals, aliquots of 2 mL of the medium were withdrawn, filtered through a 0.45-μm membrane and analyzed by the HPLC method mentioned above; however, using analytical curves obtained with the release medium (PBS at pH 7.4, 6.6, or 5.4) as diluents. At the same scheduled times, an equal volume of fresh medium was added to maintain the sink conditions. The release of the free drug was also investigated in the same way. The in vitro release studies were conducted in triplicate, and DOX cumulative release was calculated as a function of the time.

The released concentrations were plotted in the Korsmeyer-Peppas model (Ritger and Peppas 1987), using the Scientist 2.0 software (MicroMath, USA), in order to understand the behavior of the drug release from the polymeric matrix. This model is based on the equation below, in which *Mt* and *M*∞ are absolute values of drug released at time *t* and infinity, respectively, *k* considers the geometric characteristics of the system, and *n* gives the information about the diffusional release mechanism of a drug from a polymeric device.

$$kt^n = \frac{Mt}{M\infty}$$

Stability study

NPs were freshly prepared and characterized as described previously. After the first evaluations, the stability of these suspensions for the same parameters was monitored through 28 days at room temperature and

protected from the room light. In addition, the NPs capacity to remain stable at low temperature (2–8 °C) also was verified.

Lyophilization of the NP suspensions

The NP suspensions DOX-PLGA-NPs, PLGA-NPs, and Tf-DOX-PLGA-NPs were submitted to lyophilization process to obtain dried formulations (Scheeren et al. 2016). Two different cryoprotectants were tested to avoid aggregation of NPs: lactose (10%, weight of sugar per volume of NP suspension, w/v) and trehalose (10% and 15%, w/v). The cryoprotectant was solubilized in the NP aqueous suspension under magnetic stirring for 20 min and then frozen at − 20 °C during 48 h, followed by 48 h of freeze-drying (Liotop L101, Liobras, São Carlos, Brazil). The solid samples were evaluated for macroscopic appearance, physicochemical properties, and EE%.

Safety profile

The safety profile of the NP suspensions was evaluated by different blood compatibility studies, including the hemolysis assay, the erythrocyte agglutination image test (Invitox Protocol 37 1992; Nogueira et al. 2013) and the coagulation tests of prothrombin time (PT) and activated partial thromboplastin time (APTT) (Fornaguera et al. 2015). Human voluntaries were invited according to the guidelines established by the Ethics Committee in Research, from the Federal University of Santa Maria, Brazil (protocol CAAE 95038618.0.0000.5346). Erythrocytes were isolated from human blood after collection by venipuncture in EDTA tubes, following centrifugation and PBS pH 7.4 washing cycles (Nogueira et al. 2011a). Twenty-five microliter aliquots of the final erythrocyte suspension were exposed to DOX-PLGA-NPs, Tf-DOX-PLGA-NP, and free DOX at concentrations of 50, 10, and 150 μg DOX/mL and to PLGA-NPs using the same dilution volumes to ensure contact with equal concentration of the other NP components. All the samples were diluted with PBS pH 7.4 simulating the normal conditions of the blood circulation and incubated at room temperature under gentle stirring for 5 h. Then, the samples were centrifuged to stop the contact, and the supernatants were quantified at 540 nm (UV-1800 Spectrophotometer, Shimadzu, Japan). The sample absorbance was discounted from the control for each concentration without blood (negative control) and was compared with the 100% hemolysate sample prepared with water (positive control). For the erythrocyte agglutination studies, 10 μL of the each sample, after the incubation time (before the centrifugation), was placed on a glass slide, covered by a cover slip, and analyzed by a phase contrast microscope (Olympus BX41, Olympus, Japan,) with an Olympus XC50 camera and Cell Imaging software.

The PT and APTT tests were performed with fresh plasma, according to Neun and Dobrovolskaia (2010), with slight adaptations in order to promote the contact of the plasma with 150 μg/mL of DOX, coinciding with the highest concentration of hemolysis assay. For PT assessment, 200 μL of the phospholipid calcium thromboplastin were added to 100 μL of the mixture of plasma and sample, and for APTT, 100 μL of cephalin and 100 μL of calcium chloride were added. The measurement of the coagulation time was made using a Coagulometer KCl.

pH-dependent activity

The pH-dependent membrane-lytic activity of the NPs was assessed using erythrocytes as a model of the endosomal membrane (Invitox Protocol 37, 1992; Nogueira et al. 2011a). The same concentrations of free DOX and DOX-loaded NPs were added to the erythrocytes, suspended in PBS buffer at pH 7.4, 6.6, or 5.4, and exposed during 1 h and 5 h. The ability of the DOX-PLGA-NPs w/o 77KS to promote hemolysis was also measured. The negative controls were prepared in the same way for each pH. The extending and kinetic of the hemolysis was verified by the absorbance of the hemoglobin released in supernatants at 540 nm (UV-1800 Spectrophotometer, Shimadzu, Japan) in comparison with the positive control totally hemolysate in water.

Cytotoxicity assays

The tumor cell line HeLa (human epithelial cervical cancer) and the non-tumor cell line HaCaT (spontaneously immortalized human keratinocytes) were cultured in DMEM medium (4.5 g/L glucose) supplemented with 10% (v/v) FBS, 2 mM L-glutamine, 100 U/mL penicillin, and 100 μg/mL streptomycin at 37 °C in a 5% CO_2 atmosphere. These cells were routinely cultured and harvested using trypsin-EDTA when the cells reached about 80% confluency.

HeLa (1×10^5 cells/mL) and HaCaT (8.5×10^4 cells/mL) were seeded into the 96-well cell culture plates DMEM 10% FBS. Cells were incubated for 24 h under 5% CO_2 at 37 °C, and then the spent medium was replaced by DMEM 5% FBS containing the treatments DOX-PLGA-NPs, Tf-DOX-PLGA-NPs or free DOX at concentrations 0.05, 0.1, 0.25, 0.5 and 1.0 μg DOX/mL. For the unloaded-PLGA-NPs, the same dilution volumes were used to ensure contact with equal concentration of the other NP components. Each concentration were tested in triplicate and control cells were exposed to medium with 5% (v/v) FBS only. The cells were exposed for 24, 48, and 72 h to the treatment, and the resulting viability was assessed by 2,5-diphenyl-3,-(4,5-dimethyl-2-thiazolyl)tetrazolium bromide (MTT) endpoint.

MTT (0.5 mg/mL in DMEM without FBS) was added to the cells after treatment withdrawal, followed by 3 h of incubation. Finally, the MTT was removed, and 100 μL of DMSO was added to each well to dissolve the purple formazan product. After shaking, the absorbance was measured at 550 nm (Tecan microplate reader, Magellan Software V. 6.6). Cell viability was calculated as the percentage of tetrazolium salt reduced by viable cells in each sample concentration and reflects the cell metabolic activity.

Statistical analyses

Results were expressed as mean ± standard error (SE), and the statistical differences of the data were performed using one-way analysis of variance (ANOVA), followed by Tukey's or Duncan post hoc tests for multiple comparisons, using SPSS® software (SPSS Inc., Chicago, IL, USA). A p value < 0.05 was considered statistically significant.

Results

Preparation and characterization of the NPs

The NP suspensions containing or not the drug were successfully obtained and macroscopically appeared as an intense orange color and slightly whitish homogeneous liquid, respectively. The mean hydrodynamic size, polydispersity index (PDI), zeta potential (ZP), and the pH of the designed formulations are exposed in Table 1.

The TEM morphological analysis showed nanoparticles with spherical shape and regular surface (Fig. 1). The mean particle size observed by this test was 55.62 ± 1.64 nm, 51.41 ± 5.87 nm, and 53.60 ± 5.23 nm for PLGA-NPs, DOX-PLGA-NPs, and Tf-DOX-PLGA-NPs, respectively.

The HPLC method used to quantify the DOX into the NPs suspensions was validated and was found to be specific, linear in the concentration range of 1–30 μg/mL ($r = 0.9999$), accurate (100.27%), precise (relative standard deviation < 1.5%) and robust (relative standard deviation < 1%). Thus, the method was suitable to indicate the EE% result as 87.37 ± 2.81% to DOX-PLGA-NPs, as well as the drug content as 0.89 ± 0.05 mg/mL and 0.29 ± 0.02 mg/mL for DOX-PLGA-NPs and Tf-DOX-PLGA-NPs, respectively (theoretical value of 1 mg/mL).

To quantify the protein conjugation rate, three analytical curves of Tf were constructed using the Bio-Rad® assay kit in the range from 0.0375 to 0.75 mg/mL. After the spectrophotometric measurements, the average of the three analytical curves resulted in the equation $y = 0.0011x + 0.0272$, with a suitable linear correlation coefficient ($r = 0.9985$), evidencing the suitability of the analytical procedure to determine the Tf content that effectively conjugated to the NPs. From this procedure, the Tf concentration in the NPs ($n = 3$) was 0.55 ± 0.13 mg/mL, corresponding to about 38% of the theoretical concentration initially added to prepare the Tf-DOX-PLGA-NPs.

Fourier-transformed infrared spectroscopy

The FTIR spectra of each sample are showed in Fig. 2. The characteristic peak of PLGA (Fig. 2b) at 1760 cm^{-1} is due to the lactone vibration (Montha et al. 2016) and was maintained in DOX-PLGA-NPs and Tf-DOX-PLGA-NPs (Fig. 2d and e, respectively) possibly indicating the nanostructure formation. The pure DOX (Fig. 2a) spectrum shows peaks at 2933(C-H) and 1072 cm^{-1} (C-O), as found in our previous work (Scheeren et al. 2016). For the Tf-DOX-PLGA-NPs spectrum, these peaks are slightly shifted to 2927 and 1078 cm^{-1} (Fig. 2d) and for the DOX-PLGA-NPs, to 2932 and 1083 cm^{-1} (Fig. 3e), respectively. Characteristics bands of Tf protein are described elsewhere as 1648 and 1543 cm^{-1} (amide I and amide II, respectively) (Frasco et al. 2015; Soe et al. 2019). Here, these bands are presented at 1655 and 1536 cm^{-1} (Fig. 2c),

Table 1 Physicochemical characterization of the NP suspensions

	Size (nm) ± SD	PDI ± SD	ZP (mV) ± SD	pH ± SD
PLGA-NP	99.5 ± 0.5	0.22 ± 0.01	− 2.77 ± 0.31	6.73 ± 0.50
DOX-PLGA-NP	92.5 ± 0.8	0.18 ± 0.02	− 3.33 ± 0.02	6.25 ± 0.08
Tf-DOX-PLGA-NP	107.8 ± 3.8	0.20 ± 0.02	− 2.38 ± 0.63	6.25 ± 0.12

All samples were measured in triplicate. Results are expressed as the mean ± standard deviation (SD) of three experiments

and in the spectrum of Tf-DOX-PLGA-NPs appeared shifted to 1650 and 1455 cm^{-1}, respectively. The infrared spectrum of 77KS was presented elsewhere, with strong bands of carboxylate ion at 1550 and 1414 cm^{-1} (Scheeren et al. 2016). Moreover, this surfactant has an intense band at 1650 cm^{-1} region due the amide II. To evidence its presence in DOX-PLGA-NPs (Fig. 2e), these representative peaks appeared at 1641 cm^{-1} and 1400 cm^{-1}. In contrast, for the Tf-DOX-PLGA-NPs, the band of 77KS at 1650 cm^{-1} cannot be used to evidence its presence because it overlaps with vibrations of Tf protein. Trehalose presented a broad band at 3500–3200 cm^{-1} assigned to OH stretching vibration (data not shown).

In vitro DOX release

The drug release study was performed satisfying the *sink* condition, as exposed in Fig. 3. After 24 h of experiment, about 60% of the drug was released from the DOX-PLGA-NPs at PBS pH 5.4 release medium ($p < 0.05$) and smaller amounts at PBS pH 6.6 and 7.4 release media (38% and 30%, respectively). Tf-DOX-PLGA-NPs showed a similar pH-sensitive behavior, also with a visual distinction at the PBS pH 5.4, in which there was 22% of drug released, but no significant difference was observed from the pH 7.4 and 6.6. The controlled release of DOX from the NPs was compared to the free drug, which, in a nonspecific manner, made available to the PBS pH 7.4 release medium 50% of the DOX within 4 h, while the DOX-PLGA-NPs and Tf-DOX-PLGA-NPs release just 23% and 17% of the associated drug in the same experimental condition, respectively.

Release mechanism

Considering the NPs as spherical polymeric structures in a monodisperse system and knowing the values established for the exponent *n*, DOX-PLGA-NPs exhibited a diffusion-controlled drug release, that is, Fickian diffusion, in the release media PBS pH 7.4, 6.6, and 5.4, with $n = 0.28$, 0.31, and 0.35, respectively. In the same way, Tf-DOX-PLGA-NPs showed a Fickian diffusion, with $n = 0.11$, 0.098, and 0.15 for the same release media.

Stability assessment

The designed NPs were evaluated for their ability to maintain the physicochemical characteristics at room temperature and under refrigeration during a 28-day incubation period. The PLGA-NPs, DOX-PLGA-NPs, and Tf-DOX-PLGA-NPs ($n = 3$) were analyzed at time

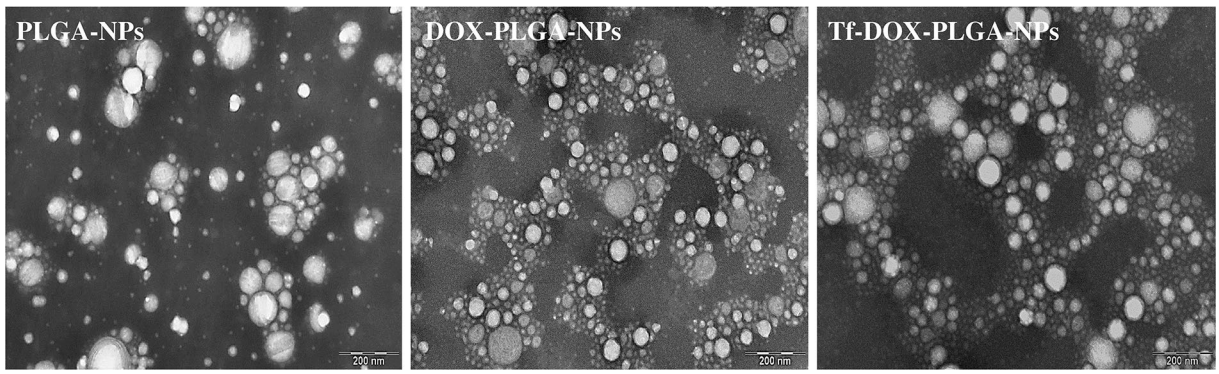

Fig. 1 TEM images of the NPs

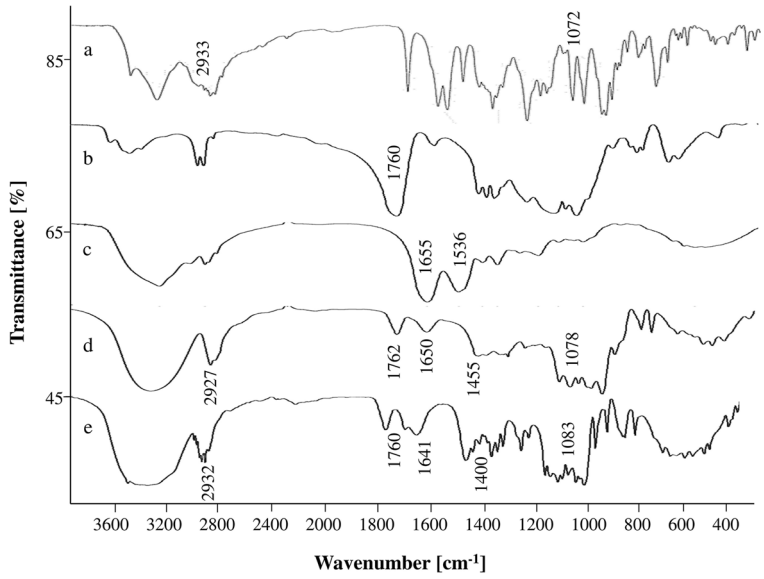

Fig. 2 FTIR spectra of DOX (a), PLGA (b), Tf (c), Tf-DOX-PLGA-NP (d), and DOX-PLGA-NP (e)

zero (immediately after preparation, T0), 7th, 14th, 21st, and 28th day. All of them showed a decrease in the pH value, in the range of 6.25 ± 0.08 to 5.37 ± 0.37, independently on the drug or protein presence. The ZP remained in the range of − 2.76 ± 0.45 to − 6.77 mV ± 0.25. Table 2 shows the increase in the mean hydrodynamic size of the DOX-PLGA-NPs and Tf-DOX-PLGA-NPs. The PLGA-NPs also exhibited a slight augment in size from 91.07 ± 0.59 to 94.42 ± 1.30. Despite the increase in size, it should be mentioned that the PDI remained below 0.30 for all of them. For both DOX-loaded NP suspensions, it was found a mild and gradual decline in the drug content. Likewise, DOX-PLGA-NPs and Tf-DOX-PLGA-NPs revealed reduction in the DC and EE%, as well as in the Tf conjugation rate. When under refrigeration, the NPs exhibited an anomalous behavior, with gelatinous appearance after 2 days, making it impossible to follow the stability study.

Lyophilization of the NP suspensions

As mentioned, the NP suspensions exhibited some variations in their physicochemical characteristics along the storage time and, therefore, it is necessary to find a way to extend their stability. In this context, the lyophilization

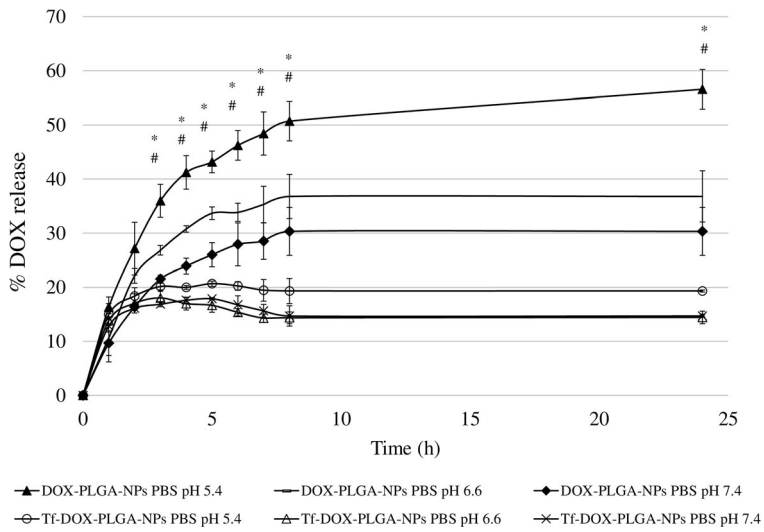

Fig. 3 Drug release profiles of DOX from the NPs. The results were analyzed by one-way ANOVA ($p < 0.05$), followed by the Tukey's post hoc test and are expressed as mean ± SE ($n = 3$). (*) and (#) denotes, respectively, significant difference of the DOX-PLGA-NPs in PBS pH 5.4 from the DOX-PLGA-NPs in PBS pH 6.6 and DOX-PLGA-NPs in PBS pH 7.4

Table 2 Physicochemical characterization of the NP suspensions throughout the period of the stability study at room temperature

	Time (days)	Size ± SD (nm)	DC ± SD (mg/mL)	EE ± SD (%)	Tf ± SD (mg/mL)
DOX-PLGA-NPs	0	91.73 ± 0.81	0.89 ± 0.03	87.44 ± 2.81	–
	7	103.06 ± 3.23	0.87 ± 0.02	80.36 ± 5.83	–
	14	100.49 ± 1.93	0.85 ± 0.03	78.14 ± 3.08	–
	21	109.90 ± 1.70	0.82 ± 0.03	76.40 ± 3.11	–
	28	123.20 ± 4.43	0.72 ± 0.03	66.02 ± 2.46	–
Tf-DOX-PLGA-NPs	0	97.74 ± 0.31	0.29 ± 0.02	–	0.57 ± 0.02
	7	115.95 ± 4.88	0.28 ± 0.01	–	0.41 ± 0.01
	14	124.95 ± 0.35	0.24 ± 0.01	–	0.37 ± 0.02
	21	133.10 ± 9.33	0.24 ± 0.04	–	0.34 ± 0.02
	28	140.25 ± 2.19	0.19 ± 0.01	–	0.34 ± 0.02

Results are expressed as the mean ± standard deviation (SD) of three experiments

process was chose as a promising approach and, among the tested cryoprotectants lactose and trehalose, the second one, at 10% (w/v), was the most suitable to protect the NPs in the freezing and desiccation stages. The freeze-dried samples had an aspect of thin untied powder and orange when DOX was present. The dried samples was resuspended with ultrapure water for the characterization analysis, applying 1 h of slight stirring followed by 15 min of sonication. The freeze-dried PLGA-NPs, DOX-PLGA-NPs, and Tf-DOX-PLGA-NPs displayed a mean hydrodynamic size of 115.1 ± 1.17 nm, 163.65 ± 1.60 nm, and 155.0 ± 2.63 nm, respectively. The PDI was < 0.30 for all NP suspensions. Thereafter, the redispersibility index was calculated as the ratio between the size of the freeze-dried NP and that of the respective NP suspension. Satisfactory values of 0.95, 1.37, and 1.07, respectively, were achieved, since the values close to 1.0 indicate a good relation between the initial and final size of the NPs. Moreover, freeze-dried DOX-PLGA-NPs showed a drug content of 0.916 mg/mL and EE% of 82.94%, while the freeze-dried Tf-DOX-PLGA-NPs, displayed a drug content of 0.346 mg/mL.

Blood compatibility and coagulation function

The release of hemoglobin from the erythrocytes was used to measure the potential of NPs to induce hemolytic damaging. Both PLGA-NPs and Tf-DOX-PLGA-NPs were biocompatible with RBC without causing hemolytic effects, as can be seen at Fig. 4a (0.74% and 0.15% in the highest concentration, respectively). In the same way, DOX-PLGA-NPs were compatible in the concentrations of 50 and 100 μg/mL (0.46 and 1.83% of hemolysis, respectively). However, a higher hemolytic rate was found for DOX-PLGA-NPs at 150 μg/mL (6.46%). In the erythrocyte agglutination image test, all the NP suspensions appeared to be non-hemolytic, as well as did not promote the agglutination of the erythrocytes, even at the highest concentration tested (Fig. 4c and e). The PT and the APTT results for the free DOX, DOX-PLGA-NPs, and Tf-DOX-PLGA-NPs were compared against the PBS control and were not significantly different. The results are exposed in Fig. 4b.

pH-dependent membrane-lytic activity

The hemolysis assay test, with the erythrocyte as a model for the endosomal membrane, was used to demonstrate the pH-dependent membrane lytic activity of unloaded- and DOX-loaded NPs. As a first step of the study, we verified the ability of DOX-loaded NPs without 77KS to promote membrane lysis as a function of pH. After 1 h of incubation, these NPs did not exhibit enhanced membranolytic activity in acidic pH, characteristic of the endosomal compartments; conversely, they promoted almost 20% of hemolysis as the pH increased to 6.6 and 7.4. As can be seen in Fig. 5a, this value rose up to 81.8% at physiological conditions after 5 h incubation. The nonencapsulated DOX showed negligible membrane lysis at the entire pH range and incubation time tested.

On the other hand, DOX-loaded NPs containing 77KS displayed a clear membranolytic activity as a function of pH reduction, regardless of the presence of the drug. At pH 7.4, 12% of hemolysis was observed after 1 h incubation with DOX-PLGA-NPs and 1% with

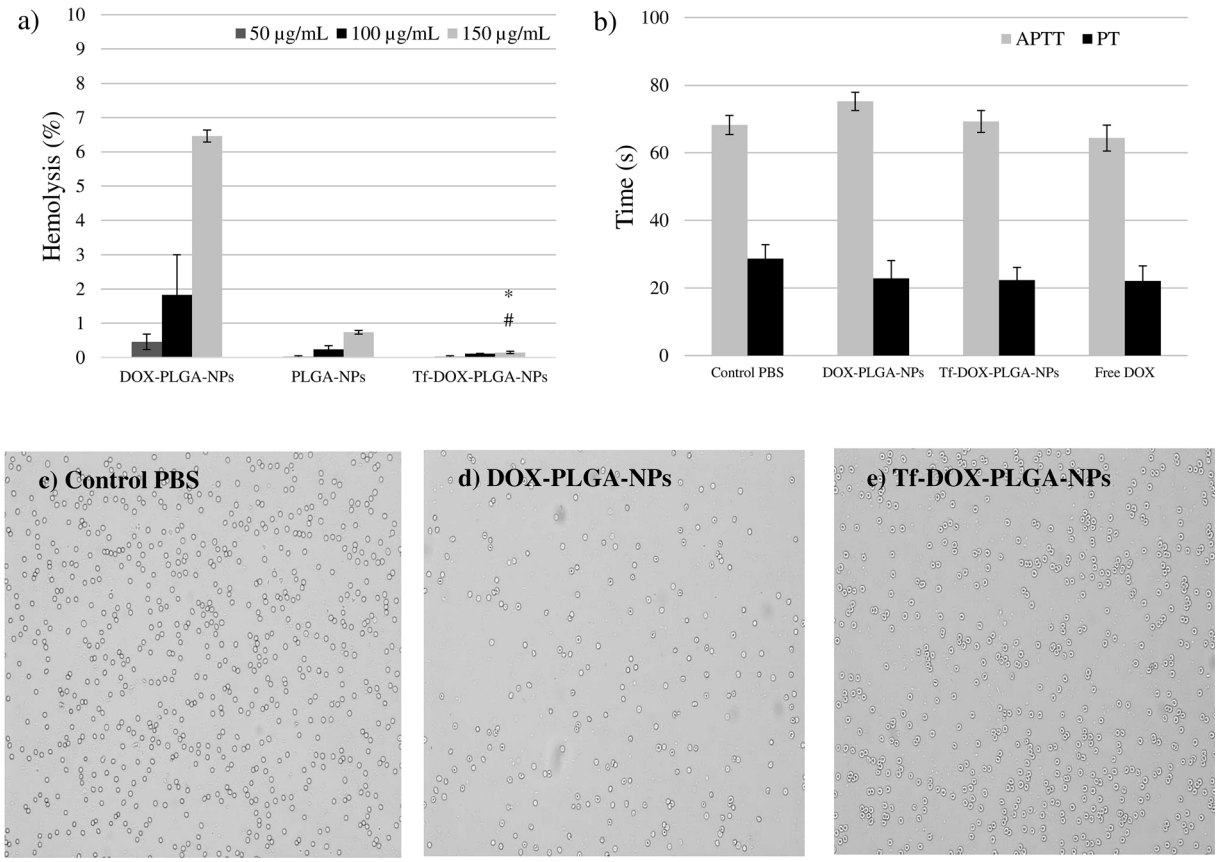

Fig. 4 Hemocompatibility studies of the NP suspensions at different concentrations after 5 h of exposition. **a** Percentage of hemolysis promoted in human erythrocytes. **b** Effects of the NPs on the plasma coagulation time PT and APTT. **c**, **d**, and **e** Agglutination test of the human erythrocytes observed by optical microscopy with PBS (negative control) or NPs at 150 µg DOX/mL. (*) Significant difference from PLGA-NPs and (#) significant difference from DOX-PLGA-NPs at same concentration, analyzed by one-way ANOVA ($p < 0.05$) followed by the Tukey's post hoc test ($n = 3$)

PLGA-NPs, while rates of 89% and 61% was achieved at pH 5.4, respectively, which means a 7.4- and 60-fold greater hemolytic rate at acidic conditions. In addition, Fig. 5 b–d showed the hemolysis of the NPs with 77KS after 5 h of incubation. In this case, the highest concentration tested for DOX-PLGA-NPs promoted 6.46% of hemolysis at pH 7.4, and as the pH decrease to 6.6 and 5.4, the membrane lytic activity increased significantly ($p < 0.05$) to 12.21% and 90.98%, representing an augment of 1.89- and 14.08-fold, respectively, in the hemolytic capacity (Fig. 5b). Likewise, PLGA-NPs (Fig. 5c) were 120-fold more membranolytic in the environment simulating the late endosomes of the tumor cell than at physiological pH ($p < 0.05$). Finally, the pH-sensitivity of the Tf-DOX-PLGA-NPs was also remarkable, but in a lesser extent (Fig. 5d). Hemolytic activity at pH 5.4 was significantly higher than at pH 6.6 and 7.4 ($p < 0.05$), with maximum hemolysis of 40.32, 4.70, and 4.86% at 150 µg/mL, respectively.

Cytotoxicity assays

The results of the cytotoxicity assays determined by the MTT endpoint are represented in Fig. 6. No significant change in viability was observed in the HaCaT and HeLa cells when treated with PLGA-NPs, suggesting the safety of this polymeric nanocarrier for drug delivery applications. In contrast, Tf-DOX-PLGA-NPs, DOX-PLGA-NPs, and free DOX solution reduced the cell viability in a time- and concentration-dependent manner. The results appeared more evident from 48 h, where the activity of the Tf-DOX-PLGA-NPs against HeLa cells is higher than both the NP formulation without the protein and the non-associated drug ($p < 0.05$). In this

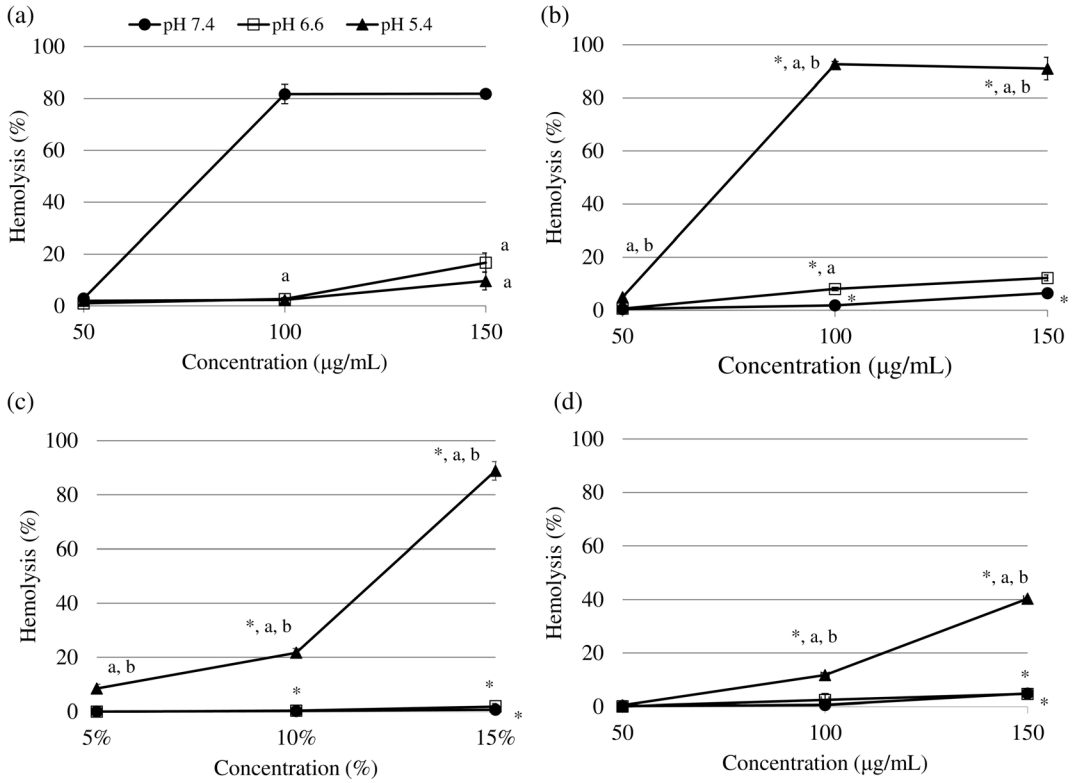

Fig. 5 pH-sensitive membrane-lytic activity of the NPs as a function of pH and concentration after 5 h of incubation. **a** DOX-PLGA-NPs w/o 77KS. **b** DOX-PLGA-NPs. **c** PLGA-NPs. **d** Tf-DOX-PLGA-NPs. *significantly different from DOX-PLGA-NPs w/o 77KS, [a]significantly different from the pH 7.4 and [b]from the pH 6.6. Statistical analyses were performed using ANOVA ($p < 0.05$) followed by Tukey's multiple comparison test. Results are expressed as mean ± SE ($n = 3$)

case, the IC_{50} of Tf-decorated NPs was 0.18 μg/mL, while the value for the DOX-PLGA-NPs and free DOX were, respectively, 0.39 μg/mL and 0.45 μg/mL. These data representing approximately a twofold increase in the toxicity of the Tf-conjugated NPs. This effect is even more remarkable after 72 h of incubation, where the cytotoxicity of the free DOX and DOX-PLGA-NPs are similar (65.1% and 64.8% of cell viability, respectively, at 0.05 μg/mL; $p > 0.05$), while the Tf-DOX-PLGA-NPs are significantly more efficient to kill the tumor cells (31.6% of cell viability at same concentration; $p < 0.05$). When the viability assay was performed with the non-tumor cell line HaCaT, noteworthy was the greater cytotoxic effects of the non-associated DOX, which reduced the cell growth in an excessive manner, maintaining only 18.8% of viable cells after 72 h at 0.05 μg/mL. On the other hand, it can be seen the effectiveness of the Tf-conjugated NPs to protect these non-tumor cells against the DOX unspecific toxicity, as 60.17% of cell viability was achieved after the same incubation time and DOX concentration (3.2-fold less cytotoxicity).

Discussion

The decision about the best treatment for cancer is quite difficult, and thus, progress is still needed to achieve successful treatment options and reduce the cancer mortality even further (Flatley and Dodwell 2019). The conventional chemotherapy exhibits few problems, such as the lack of effective delivery of the therapeutic regimens exclusively to the tumor and at ideal concentration (Cryer and Thorley 2019). The antineoplastic antibiotic DOX can reach a variety of subcellular compartments due to its amphoteric characteristic. This phenomenon is not restricted to cancer cells, and for this reason, there is a strong hypothesis about DOX-associated cardiotoxicity with possible progression to cardiomyopathy (Gewirtz 1999; Luu et al. 2018). So,

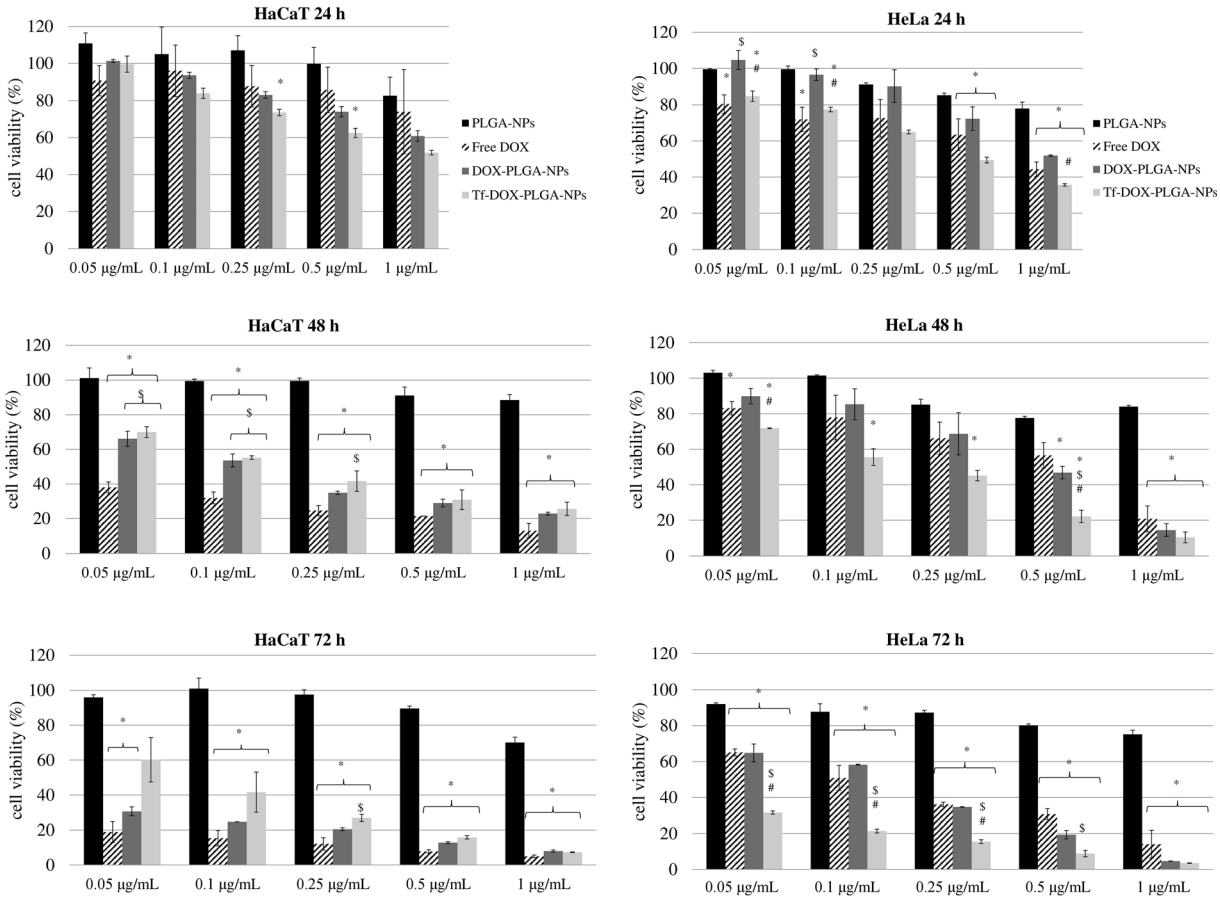

Fig. 6 Cell viability of HeLa and HaCaT cell lines with different DOX concentrations determined by MTT assay after 24, 48, and 72 h. *Significantly different from PLGA-NPs, $from the free DOX, and #from DOX-PLGA-NPs. Statistical analyses were performed using ANOVA ($p < 0.05$) followed by Duncan multiple comparison test. Results are expressed as mean ± SE ($n = 3$)

this study presents for the first time, the synergistic association of the surfactant 77KS, a pH-sensitive adjuvant well reported in the scientific literature (Nogueira et al. 2011a, 2011b; Nogueira-Librelotto et al. 2016; Scheeren et al. 2016), and the Tf protein, in a PLGA-based nanoparticle platform designed to encapsulate DOX and improve its biological activity and safety profile. Moreover, to stabilize the formulation, as well as to provide advantage in treatment of MDR cells, poloxamer was added. Besides the well documented ability of this copolymer to overcome MDR effect (Batrakova and Kabanov 2008; Swider et al. 2018), it was recently reported that its presence in DOX-loaded PLGA nanoparticles contributed to the reduction of cardiotoxicity in rabbits (Pereverzeva et al. 2019).

The DOX-PLGA-NPs were prepared following the nanoprecipitation method (Fessi et al. 1989). To control the DOX polarity, promote its lipophilicity, and maximize the entrapment efficiency, the pH of the aqueous phase was adjusted to 8.5. The DOX affinity to the organic phase increases when the pH of the aqueous phase increases from 4.0 to 9.0; however, some caution should be taken since DOX suffer degradation in pH values higher than 9.0 (Chittasupho et al. 2014; Tewes et al. 2007). The adjuvants 77KS and Tf were included in the formulation in different steps. Firstly, the surfactant was included in the aqueous phase, previously to the formation of the NP structure. Secondly, after the initial preparation process, Tf was conjugated to the surface of DOX-PLGA-NPs via amide bond formation through a two-step EDC/NHS activation and surface-grafting method (Cui et al. 2013) (Fig. 7). This conjugation reaction is based on carbodiimide reagent, the EDC, which reacts with a carboxyl end-group of the PLGA forming an amine-reactive intermediate as an activation process of these groups. At the same time,

the NHS has the role of avoiding any undesirable secondary reactions and the amine reactive is transformed in an NHS-ester derivative. When in presence of Tf, the primary amine of this protein immediately reacts with the ester along with the liberation of the NHS, resulting in the formation a PLGA-ligand conjugate (Sharma et al. 2016).

The results of the characterization by DLS showed nanometric particle size close to 100 nm, with a narrow distribution. There was a small increase in the hydrodynamic size of the Tf-DOX-PLGA-NPs, but with no significant difference, as well as found previously (Frasco et al. 2015; Tavano et al. 2014). The TEM analyses displayed NPs with smaller average diameter than those determined from DLS. This could be due to the absence of the solvation layers in the dry environment present during the TEM measurements (Montha et al. 2016). Regarding to the ZP, the values remained around −2.8 mV. This negative value is expected due to the carboxylic acid end groups of the PLGA; however, in this case, the positive charge of DOX may be interfering with the total charge of the drug-loaded NPs (Pandey et al. 2016), as well as the presence of the nonionic surfactants poloxamer and sorbitan monooleate (Betancourt et al. 2007).

Regarding to the DC into the DOX-PLGA-NPs, it was considered close to the theoretical value (1 mg/mL), while for the Tf-DOX-PLGA-NPs, this value was much lower, probably because of the extensive and detailed preparation process, which might lead to a significant drug loss. The EE% of the DOX-PLGA-NPs was considered satisfactory and is in accordance with other publications (Betancourt et al. 2007; Malinovskaya et al. 2017). Soe et al. (2019) describe a slight decrease in EE% and DC for the Tf-conjugated NPs due to leaching of the drug during the conjugation of Tf and incubation process. Chittasupho et al. (2014) report that the EE% reduced about 30% after conjugation of a transmembrane G protein antagonist (LFC131) to the NPs, justifying by the release of the drug adsorbed on the nanoparticle surface. A wide range of EE% results for DOX in Tf-modified nanoparticulated platforms is available elsewhere (Cui et al. 2013; He et al. 2017; Tavano et al. 2014); however, it is worth mentioning that in some cases, it is unclear whether there is a difference of the EE% obtained for the Tf-modified and unmodified formulations, as no data were reported for the nonconjugated NPs, hindering thus the complete interpretation of the results.

The protein conjugation can be characterized by qualitative techniques (Balasubramanian et al. 2013; Cui et al. 2013; Frasco et al. 2015) or quantitative (Chang et al. 2009; Frasco et al. 2015). Here, we did not see changes in mean size, PZ, or shape of the NPs with and without Tf, but we have achieved interesting results about the protein conjugation rate by other two assays: the colorimetric test and FT-IR analysis. The spectra showed characteristics bands of the PLGA, DOX, 77KS, and especially of the Tf slightly rearranged without abrupt changes in the structural conformation, indicating, thus, the formation of the NP matrix. Likewise, the Bio-Rad® assay proved quantitatively the Tf conjugation. Together, these data suggest that PLGA-NPs were indeed surface modified.

The NP suspensions stability was monitored during 28 days at room temperature. PLGA is known to suffer hydrolytic degradation when in aqueous medium, resulting in a decrease of the molecular weight of the polymer and generation of glycolic and lactic acids, justifying the pH reduction of the NP suspensions (Sharma et al. 2016). As observed for the DOX-PLGA-NPs, the Tf-conjugated NPs showed alterations in the physicochemical characteristics in comparison to the initial data. This same behavior was reported elsewhere for Tf-conjugated NPs after 12 days of storage (Chang et al. 2009). In this case, the Tf rate reduction can be either related to the detachment of the protein

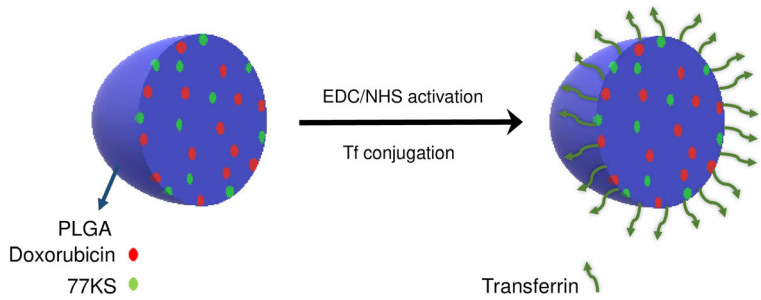

Fig. 7 Design and construction of Tf-DOX-PLGA-NPs

from the NPs or to the Tf degradation by the acidification of the suspensions caused by the polymer hydrolysis. To circumvent this loss of stability, the freeze-drying process was found as a convenient strategy. Following the optimized conditions with trehalose, we obtained suitable freeze-dried formulations, and thus, we can infer that these dried samples will have a longer stability than the NP suspensions. However, further detailed stability studies of this formulation should be carried out.

It is undeniable that the in vitro tests have been successfully explored to evidence the advantages of many ligand-targeting nanoparticulated drug delivery systems. For this reason, it is extremely important to carry out the maximum number of in vitro tests to further explore the NPs, their therapeutic and toxicological potential. Next step would be the transposition to in vivo methods, which are fairly complex and have a wide number of barriers to the delivery of NPs, promoting a gap between in vitro and in vivo research (Sriraman et al. 2016). However, before being given any clinical potential, it is imperative the comparative and complementary exploration of these two stages during the study of new formulations.

The in vitro release studies were performed at PBS pH 7.4, 6.6, and 5.4. A pH-dependent behavior was observed for DOX-PLGA-NPs, with a higher DOX cumulative release at pH 5.4 ($p < 0.05$) and pH 6.6 than at pH 7.4. The faster DOX release is related mainly to factors such as the hydrolytic destruction of the PLGA and the greater DOX solubility at acidic environment (Malinovskaya et al. 2017; Montha et al. 2016). Likewise, the role of the surfactant 77KS as a pH-sensitive adjuvant to improve the drug release has been previously described for DOX-loaded chitosan NPs (Scheeren et al. 2016). It is noteworthy the reduction in the drug release rate from Tf-DOX-PLGA-NPs. This same behavior was also described for others Tf-conjugated NPs and may be due to the surface-shielding effects by protein outer layer formation that hinders hydration of the particle, resulting in a lower diffusion of the drug to the medium (Frasco et al. 2015; Soe et al. 2019). The lower release of the drug from this nanostructure may be highly beneficial in enhancing long-term anticancer efficiency and improving drug accumulation at the targeted site (Cui et al. 2013). The drug release mechanism at the different pH values were analyzed according Korsmeyer-Peppas model. For spherical particles, n value ≤ 0.43 or ≥ 0.85, corresponds to the Fickian diffusion mechanism or case II type transport (polymer swelling), respectively, while n between 0.43 and 0.85 represents the anomalous transport (Ritger and Peppas 1987). From the results obtained, both NPs suspensions showed a release mechanism according to Fickian diffusion.

In vitro hemolysis test at physiological condition was carried out to evaluate the hemocompatibility of the NPs, as they are intended to be administered intravenously. According to the literature, permissible hemolysis values for biomaterials should be between 1 and 5% (Singhal and Ray 2002). Considering that the Tf is a protein with normal occurrence in the blood stream, together with the high biocompatibility of the PLGA and the low toxicity of the surfactant 77KS, it was necessary 5 h to verify some slight degree of lysis, similarly to Wang et al. (2014). It should be mentioned that the concentration with greater hemolytic potential was 150-fold higher than the highest concentration capable of killing the HeLa tumor cells in the cytotoxic assay. Moreover, the qualitative image test showed no evidence of neither deformed cells nor erythrocyte agglutination. Finally, to confirm the safety profile of the NP suspensions, we measured the plasma PT (a parameter for the activation of the extrinsic coagulation pathway) and the APTT (parameter for the activation of the intrinsic coagulation pathway). Compared to the assay control PBS, none of the NPs promoted significant changes in coagulation time ($p > 0.05$), indicating that the extrinsic and intrinsic coagulation pathways are not affected by the NPs. It was earlier reported that negative and near-neutral charged PLGA-NPs did not exhibited any hemolysis neither consumption in the PT or APTT, while positive charged NPs showed some reduction in the APTT (Pillai et al. 2015).

The potential of the NPs to disrupt lipid bilayers membranes as a function of pH was assessed using human erythrocytes as a model for endosomal membranes. The main result to be highlighted is the greater membranolytic activity of the NPs containing 77KS as the pH of the surrounding medium decreased, especially to 5.4. In contrast, the NPs without 77KS did not show this pH-responsive activity, emphasizing once again the role of this surfactant in controlling the NP behavior according to the pH stimulus. The predominant hypothesis would be the protonation of the carboxylic group of the 77KS, making it closer to the neutrality and lipophilic form, therefore with greater capacity to interact with the membrane, modifying its permeability and

causing its lysis (Nogueira et al. 2016; Nogueira-Librelotto et al. 2016). Regarding to the Tf-conjugated NPs, it is believed that the protein coating could hinder the 77KS molecules, reducing its pH-responsive activity. Even so, it is possible to observe a pH-sensitive behavior for this NP. In addition, the differences observed in this experiment for the DOX-loaded suspensions are another indicative that the Tf is effectively assembled to the surface of the nanostructure.

Different cell models were chosen to perform this study. The HeLa tumor cells were selected due to the overexpression of TfR, while HaCaT cells was used as a non-tumor model, with low expression of these receptors (Tsuji et al. 2013; Daniels et al. 2006). DOX has unspecific and toxic effects on healthy cells, which justify the evaluation of its general cytotoxicity on a non-tumor cell line. Our results evidenced important cytotoxic effects of non-associated DOX against HaCaT cells, which is even higher than the toxic effects observed in the tumor cell line. In this same way, Kumari et al. (2018) also demonstrated noteworthy cytotoxic effects of free DOX in this same cell model (HaCaT), as well as reduction in drug toxicity after successfully loading it in a nanocarrier. Likewise, free DOX was highly cytotoxic to human umbilical vein endothelial cells (HUVEC), while this undesirable effect was partially overcome after DOX association to Tf-conjugated NPs (Tsuji et al. 2013). The DOX-PLGA-NPs also showed some effect against the HaCaT cells but not so much as free DOX, with significant difference at 48 h ($p < 0.05$). Such cytotoxicity for free DOX can be explained by its small molecular structure, diffusing into the cell more rapidly than the NPs and then inducing cellular mortality in low concentration (Montha et al. 2016; Nogueira-Librelotto et al. 2016). Some studies showed that free DOX has similar or higher cytotoxicity than PLGA NPs encapsulating DOX (Betancourt et al. 2007; Malinovskaya et al. 2017). For Montha et al. (2016), NPs were as effective as free DOX only above 250 μg/mL against HeLa cell line; at lower concentrations, the free drug was more cytotoxic. However, such high concentration of the nanosystem no longer effectively represents an advantage if transposed to in vivo methods or clinical trials, since the drug would be available to exert its effect also on non-tumor cells with consequent adverse effects. The ideal pattern would be to achieve a substantial toxic effect against tumor cells with little effect on normal cells in low concentrations of NPs, as we verified in our study with Tf-DOX-PLGA-NPs. Here, this nanoplatform deserves to be highlighted. As expected, it was the one with the greatest capacity to kill HeLa tumor cells at low concentrations after 48 h and 72 h ($p < 0.05$), and at the same time, it was the least cytotoxic against the HaCaT non-tumor cells ($p < 0.05$), indicating that the Tf-conjugated NPs have an improved selectivity toward cancer cells, with reduced unspecific cytotoxicity against healthy cells. Tf-conjugated NPs are likely to promote cumulative cytotoxic effect with a longer incubation time, which is consistent with the in vitro drug release study. The potent antiproliferative activity of the Tf-DOX-PLGA-NPs on HeLa cells is an indicative of the higher number of TfR on cancer cells and confirms the specificity of the Tf-inspired systems to these cells, in agreement with early published data (Sriraman et al. 2016; Daniels et al. 2006). These NPs are likely internalized by TfR-mediated endocytosis, and although non-tumor cells also express TfR, its expression is at a level just to maintain the normal functioning of the cell (Balasubramanian et al. 2013). Moreover, after internalization, the NPs with Tf are able to remain more time accumulated inside the cell, bypassing the effect of efflux pumps, while free DOX is rapidly eliminated (He et al. 2017; Sahoo and Labhasetwar 2005).

Conclusion

We have successfully developed a dual-active targeting nanocarrier for DOX delivery, which was based on a biocompatible and biodegradable PLGA polymeric matrix, modified with the pH-sensitive surfactant 77KS and surface-decorated with Tf protein. All suspensions were completely characterized, satisfying what is expected for a promising nanosystem. The main advantages of the Tf-DOX-PLGA-NPs include the controlled and pH-dependent drug release, the pH-responsiveness membranolytic activity, and the high blood compatibility. Moreover, Tf-conjugated NPs killed HeLa cells in a greater extent than DOX did, while they also showed much less toxicity on non-tumor HaCaT cells than DOX. Therefore, these NPs appear to be promising to diminish the unwanted side effects of the free drug. For all these reasons, we believe that this nanoplatform will be further fruitful, and more in vitro studies are in progress.

Funding information This research was supported by Projects 447548/2014-0 and 401069/2014-1 of the *Conselho Nacional de Desenvolvimento Científico e Tecnológico* (CNPq - Brazil). L.E.S thanks the *Coordenação de Aperfeiçoamento de Pessoal de Nível Superior* (CAPES) for the PhD fellowship at *Universidade Federal de Santa Maria* and CNPq for the PhD internship at *Universitat de Barcelona* (grant number 204255/2018-0). D.R.N-L. thanks CNPq-Brazil for the Postdoctoral grant (grant number 150920/2018-0).

Compliance with ethical standards

Conflict of interest The authors declare that they have no conflict of interest.

References

AbuHammad S, Zihlif M (2013) Gene expression alterations in doxorubicin resistant MCF7 breast cancer cell line. Genomics 101:213–220. https://doi.org/10.1016/j.ygeno.2012.11.009

Baker EN, Baker HM, Kidd RD (2002) Lactoferrin and transferrin: functional variations on a common structural framework. Biochem Cell Biol 80:27–34. https://doi.org/10.1139/o01-153

Balasubramanian S, Girija AR, Nagaoka Y, Iwai S, Suzuki M, Kizhikkilot V, Yoshida Y, Maekawa T, Nair SD (2013) Curcumin and 5-fluorouracil-loaded, folate- and transferrin-decorated polymeric magnetic nanoformulation: a synergistic cancer therapeutic approach, accelerated by magnetic hyperthermia. Int J Nanomedicine 9:437–459. https://doi.org/10.2147/IJN.S49882

Barenholz Y (2012) Doxil® — the first FDA-approved nano-drug: lessons learned. J Control Release 160:117–134. https://doi.org/10.1016/j.jconrel.2012.03.020

Batrakova EV, Kabanov AV (2008) Pluronic block copolymers: evolution of drug delivery concept from inert nanocarriers to biological response modifiers. J Control Release 130:98–106. https://doi.org/10.1016/j.jconrel.2008.04.013

Betancourt T, Brown B, Branon-Peppas L (2007) Doxorubicin-loaded PLGA nanoparticles by nanoprecipitation: preparation, characterization and in vitro evaluation. Nanomedicine 2:219–232. https://doi.org/10.2217/17435889.2.2.219

Bradford MM (1976) A rapid and sensitive method for quantitation of microgram quantities of protein utilizing the principle of protein-dye binding. Anal Biochem 72:248–254. https://doi.org/10.1006/abio.1976.9999

Chang J, Jallouli Y, Kroubi M, Yuan X, Feng W, Kang C, Pu P, Betbeder D (2009) Characterization of endocytosis of transferrin-coated PLGA nanoparticles by the blood–brain barrier. Int J Pharm 379:285–292. https://doi.org/10.1016/j.ijpharm.2009.04.035

Chang J, Paillard A, Passirani C, Morille M, Benoit J, Betbeder D, Garcion E (2012) Transferrin adsorption onto PLGA nanoparticles governs their interaction with biological systems from blood circulation to brain Cancer cells. Pharm Res 29:1495–1505. https://doi.org/10.1007/s11095-011-0624-1

Chittasupho C, Lirdprapamongkol K, Kewsuwan P, Sarisuta N (2014) Targeted delivery of doxorubicin to A549 lung cancer cells by CXCR4 antagonist conjugated PLGA nanoparticles. Eur J Pharm Biopharm 88:529–538. https://doi.org/10.1016/j.ejpb.2014.06.020

Cryer AM, Thorley AJ (2019) Nanotechnology in the diagnosis and treatment of lung cancer. Pharm Ther, in press. https://doi.org/10.1016/j.pharmthera.2019.02.010

Cui Y, Xu Q, Chow PK, Wang D, Wang C (2013) Transferrin-conjugated magnetic silica PLGA nanoparticles loaded with doxorubicin and paclitaxel for brain glioma treatment. Biomaterials 34:8511–8520. https://doi.org/10.1016/j.biomaterials.2013.07.075

Danhier F, Feron O, Préat V (2010) To exploit the tumor microenvironment: passive and active tumor targeting of nanocarriers for anti-cancer drug delivery. J Control Release 148:135–146. https://doi.org/10.1016/j.jconrel.2010.08.027

Daniels TR, Delgado T, Rodriguez JA, Helguera G, Penichet ML (2006) The transferrin receptor part I: biology and targeting with cytotoxic antibodies for the treatment of cancer. Clin Immunol 121:144–158. https://doi.org/10.1016/j.clim.2006.06.010

Fessi H, Puisieux F, Devissaguet JP, Ammoury N, Benita S (1989) Nanocapsule formation by interfacial polymer deposition following solvent displacement. Int J Pharm 55:R1–R4. https://doi.org/10.1016/0378-5173(89)90281-0

Flatley M, Dodwell D (2019) Adjuvant treatment for breast cancer. Surgery (Oxford) 34:43–46. https://doi.org/10.1016/j.mpsur.2015.10.003

Fornaguera C, Calderó G, Mitjans M, Vinardell MP, Solansa C, Vauthier C (2015) Interactions of PLGA nanoparticles with blood components: protein adsorption, coagulation, activation of the complement system and hemolysis studies. Nanoscale 7:6045–6059. https://doi.org/10.1039/c5nr00733j

Frasco MF, Almeida GM, Santos-Silva F, Pereira M do C, Coelho MAN (2015).Transferrin surface-modified PLGA nanoparticles-mediated delivery of a proteasome inhibitor to human pancreatic cancer cells. J Biomed Mater Res A103A:1476–1484. https://doi.org/10.1002/jbm.a.35286

Gewirtz DA (1999) A critical evaluation of the mechanisms of action proposed for the antitumor effects of the anthracycline antibiotics adriamycin and daunorubicin. Biochem Pharmacol 57:727–741. https://doi.org/10.1016/s0006-2952(98)00307-4

Hare JI, Lammers T, Ashford MB, Puri S, Storm G, Barry ST (2017) Challenges and strategies in anti-cancer nanomedicine development: an industry perspective. Adv Drug Deliv Rev 108:25–38. https://doi.org/10.1016/j.addr.2016.04.025

He Y, Xing L, Cui P, Zhang J, Zhu Y, Qiao J, Lyu J, Zhang M, Luo C, Zhou Y, Lu N, Jiang H (2017) Transferrin-inspired vehicles based on pH-responsive coordination bond to combat multidrug-resistant breast cancer. Biomaterials 113:266–278. https://doi.org/10.1016/j.biomaterials.2016.11.001

ICH – International Conference on Harmonisation of Technical Requirements for Registration of Pharmaceuticals for Human Use Q2 R1: Guideline on Validation of Analytical Procedure – Methodology. (2005)

INVITOX PROTOCOL (1992) Number 37: red blood cell test system

Kumari M, Purohit MP, Patnaik S, Shukla Y, Kumar P, Gupta KC (2018) Curcumin loaded selenium nanoparticles synergize the anticancer potential of doxorubicin contained in self-assembled, cell receptor targeted nanoparticles. Eur J Pharm Biopharm 130:185–199. https://doi.org/10.1016/j.ejpb.2018.06.030

Lee ES, Oh KT, Kim D, Youn YS, Bae YH (2007) Tumor pH-responsive flower-like micelles of poly(L-lactic acid)-b-poly (ethylene glycol)-b-poly(L-histidine). J Control Release 123: 19–26. https://doi.org/10.1016/j.jconrel.2007.08.006

Luu AZ, Chowdhury B, Al-Omran M, Teoh H, Hess DA, Verma S (2018) Role of endothelium in doxorubicin-induced cardiomyopathy. JACC Basic Transl Sci 3:861–871. https://doi.org/10.1016/j.jacbts.2018.06.005

Macedo LB, Nogueira-Librelotto DR, Vargas J, Scheeren LE, Vinardell MP, Rolim CMB (2019) Poly (ε-Caprolactone) nanoparticles with pH-responsive behavior improved the In Vitro antitumor activity of methotrexate. AAPS PharmSciTech 20:165–177. https://doi.org/10.1208/s12249-019-1372-5

Malinovskaya Y, Melnikov P, Baklaushev V, Gabashvili A, Osipova N, Mantrov S, Ermolenko Y, Maksimenko O, Gorshkova M, Balabanyan V, Kreuter J, Gelperina S (2017) Delivery of doxorubicin-loaded PLGA nanoparticles into U87 human glioblastoma cells. Int J Pharm 524:77–90. https://doi.org/10.1016/j.ijpharm.2017.03.049

Montha W, Maneeprakorn W, Buatong N, Tang I-M, Pon-On W (2016) Synthesis of doxorubicin-PLGA loaded chitosan stabilized (Mn, Zn)Fe2O4 nanoparticles: biological activity and pH-responsive drug release. Mater Sci Eng C 59:235–240. https://doi.org/10.1016/j.msec.2015.09.098

Muhamad N, Plengsuriyakarn T, Na-Bangchang K (2018) Application of active targeting nanoparticle delivery system for chemotherapeutic drugs and traditional/herbal medicines in cancer therapy: a systematic review. Int J Nanomedicine 13:3921–3935. https://doi.org/10.2147/IJN.S165210

Neun BW, Dobrovolskaia MA (2010) Method for in vitro analysis of nanoparticle thrombogenic properties. Characterization of Nanoparticles Intended for Drug Delivery. Methods Mol Biol 697 chapter 24

Nogueira DR, Mitjans M, Infante MR, Vinardell MP (2011a) The role of counterions in the membrane-disruptive properties of pH-sensitive lysine-based surfactants. Acta Biomater 7: 2846–2856. https://doi.org/10.1016/j.actbio.2011.03.017

Nogueira DR, Mitjans M, Infante MR, Vinardell MP (2011b) Comparative sensitivity of tumor and non-tumor cell lines as a reliable approach for in vitro cytotoxicity screening of lysine-based surfactants with potential pharmaceutical applications. Int J Pharm 420:51–58. https://doi.org/10.1016/j.ijpharm.2011.08.020

Nogueira DR, Tavano L, Mitjans M, Pérez L, Infante MR, Vinardell MP (2013) In vitro antitumor activity of methotrexate via pH-sensitive chitosan nanoparticles. Biomaterials 34:2758–2772. https://doi.org/10.1016/j.biomaterials.2013.01.005

Nogueira DR, Scheeren LE, Vinardell MP, Mitjans M, Infante MR, Rolim CMB (2015) Nanoparticles incorporating pH-responsive surfactants as a viable approach to improve the intracellular drug delivery. Mater Sci Eng C 57:100–106. https://doi.org/10.1016/j.msec.2015.07.036

Nogueira DR, Scheeren LE, Macedo LB, Marcolino AIP, Vinardell MP, Mitjans M, Infante MR, Farooqi A, Rolim CMB (2016) Inclusion of a pH-responsive amino acid-based amphiphile in methotrexate-loaded chitosan nanoparticles as a delivery strategy in cancer therapy. Amino Acids 48:157–168. https://doi.org/10.1007/s00726-015-2075-1

Nogueira-Librelotto DR, Scheeren LE, Vinardell MP, Mitjans M, Rolim CMB (2016) Chitosan-tripolyphosphate nanoparticles functionalized with a pH-responsive amphiphile improved the in vitro antineoplastic effects of doxorubicin. Colloid Surface B 147:326–335. https://doi.org/10.1016/j.colsurfb.2016.08.014

Nogueira-Librelotto DR, Codevilla CF, Farooqi A, Rolim CMB (2017) Transferrin-conjugated Nanocarriers as active-targeted drug delivery platforms for cancer therapy. Cur Pharm Des 23:454–466. https://doi.org/10.2174/1381612822666161026162347

Nothnagel L, Wacker MG (2018) How to measure release from nanosized carriers? Eur J Pharm Sci 120:199–211. https://doi.org/10.1016/j.ejps.2018.05.004

Pandey SK, Patel DK, Maurya AK, Thakur R, Mishra DP, Vinayak M, Haldar C, Maiti P (2016) Controlled release of drug and better bioavailability using poly(lacticacid-co-glycolic acid) nanoparticles. Int J Biol Macromol:8999–8110. https://doi.org/10.1016/j.ijbiomac.2016.04.065

Pereverzeva E, Treschalin I, Treschalin M, Arantseva D, Ermolenko Y, Kumskova N, Maksimenko O, Balabanyan V, Kreuter J, Gelperina S (2019) Toxicological study of doxorubicin-loaded PLGA nanoparticles for the treatment of glioblastoma. Int J Pharm 554:161–178. https://doi.org/10.1016/j.ijpharm.2018.11.014

Pillai GJ, Greeshma MM, Menon D (2015) Impact of poly(lactic-co-glycolic acid) nanoparticle surface charge on protein, cellular and haematological interactions. Colloid Surface B 136: 1058–1066. https://doi.org/10.1016/j.colsurfb.2015.10.047

Ritger PL, Peppas NA (1987) A simple equation for description of solute release I. Fickian and non-Fickian release from non-swellable devices in the form of slabs, spheres, cylinders or discs. J Control Release 5:23–36. https://doi.org/10.1016/0168-3659(87)90034-4

Sahoo SK, Labhasetwar V (2005) Enhanced antiproliferative activity of tranferrin-conjugated paclitaxel-loaded nanoparticles is mediated via sustained intracellular drug retention. Mol Pharm 2:373–383. https://doi.org/10.1021/mp050032z

Sanchez L, Mitjans M, Infante MR, Vinardell MP (2006a) Potential irritation of lysine derivative surfactants by hemolysis and HaCaT cell viability. Toxicol Lett 161:53–60. https://doi.org/10.1016/j.toxlet.2005.07.015

Sanchez L, Mitjans M, Infante MR, Vinardell MP (2006b) Determination of interleukin-1in human NCTC 2544 keratinocyte cells as a predictor of skin irritation from lysine-based surfactants. Toxicol Lett 167:40–46. https://doi.org/10.1016/j.toxlet.2006.08.006

Scheeren LE, Nogueira DR, Macedo LB, Vinardell MP, Mitjans M, Infante MR, Rolim CMB (2016) PEGylated and poloxamer-modified chitosan nanoparticles incorporating a lysine-based surfactant for pH-triggered doxorubicin release. Colloid Surface B 138:117–127. https://doi.org/10.1016/j.colsurfb.2015.11.049

Scheeren LE, Nogueira DR, Fernandes JR, Marcolino AIP, Macedo LB, Vinardell MP, Rolim CMB (2017) Comparative study of reversed-phase high-performance liquid chromatography and ultraviolet–visible

spectrophotometry to determine doxorubicin in pH-sensitive nanoparticles. Anal Lett 51:1445–1463. https://doi.org/10.1080/00032719.2017.1380034

Sharma S, Parmar A, Kori S, Sandhir R (2016) PLGA-based nanoparticles: a new paradigm in biomedical applications. Trends Anal Chem 80:30–40. https://doi.org/10.1016/j.trac.2015.06.014

Shen ZM, Yang JT, Feng Y, Wu CC (1992) Conformational stability of porcine serum transferrin. Prot Sci I:1477–1484. https://doi.org/10.1002/pro.5560011109

Shindelman JE, Ortmeyer AE, Sussman HH (1981) Demonstration of the transferrin receptor in human breast cancer tissue. Potential marker for identifying dividing cells. Int J Cancer 27:329–334. https://doi.org/10.1002/ijc.2910270311

Singhal JP, Ray AR (2002) Synthesis of blood compatible polyamide block copolymers. Biomaterials 23:1139–1145. https://doi.org/10.1016/S0142-9612(01)00228-9

Soe ZC, Kwon JB, Thapa RK, Ou W, Nguyen HT, Gautam M, Oh KT, Choi H, Ku SK, Yong CS, Kim JO (2019) Transferrin-conjugated polymeric nanoparticle for receptor-mediated delivery of doxorubicin in doxorubicin-resistant breast cancer cells. Pharmaceutics 11:63–80. https://doi.org/10.3390/pharmaceutics11020063

Sriraman SK, Salzano G, Sarisozen C, Torchilin V (2016) Anticancer activity of doxorubicin-loaded liposomes co-modified with transferrin and folic acid. Eur J Pharm Biopharm 105:40–49. https://doi.org/10.1016/j.ejpb.2016.05.023

Swider E, Koshkina O, Tel J, Cruz LJ, de Vries IJM, Srinivas M (2018) Customizing poly(lactic-co-glycolic acid) particles for biomedical applications. Acta Biomater 73:38–51. https://doi.org/10.1016/j.actbio.2018.04.006

Tavano L, Aiello R, Ioele G, Picci N, Muzzalupo R (2014) Niosomes from glucuronic acid-based surfactant as new carriers for cancer therapy: preparation, characterization and biological properties. Colloid Surface B 118:7–13. https://doi.org/10.1016/j.colsurfb.2014.03.016

Tewes F, Munnier E, Antoon B, Okassa LN, Cohen-Jonathan S, Marchais H, Douziech-Eyrolles L, Souce M, Dubois P, Chourpa I (2007) Comparative study of doxorubicin-loaded poly(lactide-co-glycolide) nanoparticles prepared by single and double emulsion methods. Eur J Pharm Biopharm 66:488–492. https://doi.org/10.1016/j.ejpb.2007.02.016

Thorn CF, Oshiro C, Marsh S, Hernandez-Boussard T, McLeod H, Klein TE, Altman RB (2011) Doxorubicin pathways: pharmacodynamics and adverse effects. Pharmacogenet Genomics 21(7):440–446. https://doi.org/10.1097/FPC.0b013e32833ffb56

Tian L, Bae YH (2012) Cancer nanomedicines targeting tumor extracellular pH. Colloid Surface B 99:116–126. https://doi.org/10.1016/j.colsurfb.2011.10.039

Tsuji T, Yoshitomi Y, Usukura J (2013) Endocytic mechanism of transferrin-conjugated nanoparticles and the effects of their size and ligand number on the efficiency of drug delivery. Microscopy 62:341–352. https://doi.org/10.1093/jmicro/dfs080

Vives MA, Infante MR, Garcia E, Selve C, Maugras M, Vinardell MP (1999) Erythrocyte hemolysis and shape changes induced by new lysine-derivate surfactants. Chem-Biol Interac 118:1–18. https://doi.org/10.1016/s0009-2797(98)00111-2

Wang H, Zhao Y, Wang H, Gong J, He H, Shin MC, Yang VC, Huang Y (2014) Low-molecular-weight protamine-modified PLGA nanoparticles for overcoming drug-resistant breast cancer. J Control Release 192:47–56. https://doi.org/10.1016/j.jconrel.2014.06.051

Zhang X, Li J, Yan M (2016) Targeted hepatocellular carcinoma therapy: transferrin modified, self-assembled polymeric nanomedicine for co-delivery of cisplatin and doxorubicin. Drug Dev Ind Pharm 40:1590–1599. https://doi.org/10.3109/03639045.2016.1160103